

Structural, dynamic and mechanical evolution of water confined in the nanopores of disordered calcium silicate sheets

Dongshuai Hou¹ · Cong Lu² · Tiejun Zhao³ · Peng Zhang³ · Qingjun Ding⁴

Received: 19 April 2015 / Accepted: 8 September 2015 / Published online: 30 September 2015
© Springer-Verlag Berlin Heidelberg 2015

Abstract Water molecules confined in the interlayer region of calcium silicate hydrate (C–S–H) are closely related to the cohesion in the cementitious materials. In this research, molecular dynamics is employed to investigate the structure, dynamics and mechanical properties of water molecules in the nanopore of C–S–H gels at ambient temperature. In order to consider the confinement effect of calcium silicate sheets, the pore size expressed as interlayer distance changes from 13 to 22 Å. The water molecules near the C–S–H surface are strongly influenced by the O_{NB} atoms in the silicate chains and Ca_w atoms in the interlayer region. They demonstrate following structural features: layering in the water density profile, the orientation preference in the dipolar angle distribution and long special correlation in the radial distribution function.

Dynamically, while the interlayer distance increases by 10 Å, the diffusion coefficient transfers through two orders of magnitude from 3.42×10^{-12} to $5.3 \times 10^{-10} \text{ m}^2/\text{s}^2$. In the mean square displacement curves, the cage stage, a characteristic of the dynamics in the glasses, gradually disappears with increasing interlayer distance. The dynamic evolution of water molecules is primarily induced by the changes in the strength of H-bonds and $Ca-O_w$ connections, which is consistent with lowering of the frequency in the simulated vibration spectrum. The strongly attractive interaction between water molecules and calcium silicate layer is weakened and the motion of water molecules is less restricted at large interlayer distance. Furthermore, the interlayer fluid pressure study shows that the cohesion in the C–S–H gel, contributed by the interlayer calcium atoms, progressively diminishes from 1.5 to 0 GPa, due to the enhancing disjoining effect of water molecules connected with calcium atoms with increasing interlayer distance.

✉ Cong Lu
cluab@ust.hk

Dongshuai Hou
dhou@ust.hk; monkeyphildhou@gmail.com

Tiejun Zhao
ztjgp@263.net

Peng Zhang
zhp0221@163.com

Qingjun Ding
dingqj@whut.edu.cn

Keywords Molecular dynamics · Interlayer water molecules · Dipolar angle · Mean square displacement · Fluid pressure

1 Introduction

When water reacts with the cement particles, the hydration process gives birth to the calcium silicate hydrate (C–S–H) gel, the most important binding phase in cement-based material (Li 2011). The C–S–H gel is a mesoporous material, whose solid skeleton is made of calcium silicate sheets, with water distributed in the interlayer space (Pelletier et al. 2009). The motion of water molecules confined in the nanopores is directly related to the cohesion of the

¹ Qingdao Technological University, Qingdao, China

² Department of Civil and Environmental Engineering, Hong Kong University of Science and Technology, Clear Water Bay, Kowloon, Hong Kong

³ Department of Civil Engineering, Qingdao Technological University, Qingdao, China

⁴ School of Materials Science and Engineering, Wuhan University of Technology, Wuhan, China

binding phase, which further influences the mechanical properties and durability of the cement-based materials. However, the water molecules ultra-confined in the nanopore show dramatically different physical and chemical features from that of the bulk counterpart. On the one hand, the complicated chemical compositions, such as Ca/Si and H₂O/Si ratios, result in variation of the pore size distribution and connectivity (Ma and Li 2013). Water molecules diffusing and exchanging in the nanopore are greatly influenced by the local geometry of the complicated pore structures. On the other hand, as the essential part of the C–S–H gel, the states of confined water molecules are sensitive to the surrounding environment and humidity: the C–S–H gels lose the interlayer water in case of a fire, while the gels are saturated in the water.

The properties of the water confined in gel pores, or in the vicinity of C–S–H surfaces, have been studied by various experimental techniques. By using the ¹H nuclear magnetic resonance (NMR) (Wang et al. 1998; Rakiewicz et al. 1998; Greener et al. 2000), the water in C–S–H gels has been distinguished into three types: chemically bound water that is incorporated into the structure and forms strong chemical bond with the calcium silicate structure, physical bound water that is deeply adsorbed near the surface and capillary water that is not bound and diffuses freely in the capillary pores. The quasi-elastic neutron scattering (QENS) technique (Bordallo et al. 2006) furthermore characterizes the different water types by quantitatively using the diffusion coefficient. The unbound water molecules in the pores move at a fast rate (diffusion coefficient $\sim 10^{-9}$ m²/s), while the water molecules confined in the gel pores diffuse slowly ($\sim 10^{-10}$ m²/s). Hydration water dynamics in tricalcium silicate (C₃S) pastes by QENS also showed that the diffusion coefficient of surface-adsorbed water molecules decreases from 4×10^{-9} to 4×10^{-10} m²/s after 2-day hydration. A proton field cycling relaxometry approach (PFCR), developed to investigate the dynamic properties of the water molecules bound in the C–S–H surface (Korb et al. 2007), has found that in approximately 1 ns, the diffusion coefficient of the water molecules in the C–S–H gel pore surface is about 1/60 of the bulk water value (0.4×10^{-10} m²/s).

Investigating the water structure and dynamics by experiment alone is challenged by some limitations, such as the material purity and instrument accuracy at the relevant lengths and timescales. Computational methods assist to interpret the experimental results and play a complementary role in understanding the structural and dynamic properties at the molecular level. Water molecules, the essential composition in C–S–H gel, have been investigated since the development of the “realistic model.” Pellenq et al. (2012) simulated stress–strain relation of C–S–H gel in resisting shear force. By comparing mechanical performance of the

dry and wet C–S–H gels, their research concluded that during loading process, large displacements of water molecules in wet C–S–H gel weaken shear strength and result in unrecovered deformations. Youssef et al. (2011) investigated structural and dynamic features of water molecules in the C–S–H gel and determined that due to the highly hydrophilic nature of calcium silicate sheet, H-bonds constructed between non-bridging oxygen and water is very strong. Water molecules constrained in the gel therefore demonstrate glassy nature: tetrahedral spatial structure is distorted and the diffusion rate is significantly reduced. Ji et al. (2012) utilized five classic water models including SPC, TIP3P, TIP4P, TIP4P05 and TIP5P to simulate calcium silicate hydrate. They concluded that SPC and TIP5P describe accurately the intrinsic properties of C–S–H gel and SPC (flexible) is more computationally efficient. More recently, Bonnaud et al. (2012) interpreted the cohesive force of C–S–H gel by analyzing fluid pressure of water molecules and the counter-ions in the interlayer region. Under different humidity conditions, they found that the cohesive force mainly results from negative pressure caused by the interaction between interlayer calcium atoms and calcium silicate sheets. Even though this work of Bonnaud et al. took into consideration the water amount in the C–S–H gel, it was assumed that molecular structure of calcium silicate sheet remained unchanged under different humidity conditions. This assumption, ignoring the structural evolution due to water effect, may be further improved.

In the study reported in this paper, molecular dynamics has been utilized to investigate the structure, dynamics and mechanical properties of the water molecules confined in the C–S–H gels. In order to study the effects of the calcium silicate confinement, the interlayer distance has been varied from 13 to 22 Å. In the length scale, the cohesion between neighboring C–S–H particles occurs. Simulations conducted aimed to give insight into structural and dynamic evolution of water molecules in the C–S–H gel as a function of interlayer distance. The importance of the spacing investigation is considered in two respects. Firstly, a C–S–H grain can be exposed to many different environmental conditions in terms of temperature and relative humidity RH. The intra-granular distance varies with changing of external environments. Secondly, there is a need to account for the multi-porosity nature of CSH gel. The moving of water molecules in the nanopores has great influence on the physical and chemical properties of the C–S–H gel. Since many properties of C–S–H gel are sensitive to the gel pore size at this length scale (1–2 nm), it is necessary to investigate spacing dependence. Density profiles, atomic trajectories, dipolar angle distribution and radial distribution function are employed to characterize the structural feature of confined water molecules. The dynamic properties have been investigated by analyzing the mean square displacement,

time correlated function and the van Hove relations. Additionally, the internal fluid pressure and the elastic modulus have been further studied to provide useful information on the mechanical properties of C–S–H gel.

2 Simulation method

Molecular dynamics simulations were performed using the Large-scale Atomic/Molecular Massively Parallel Simulator [LAMMPS (developed at Sandia National Laboratories)] (Plimpton 1995; Plimpton et al. 2001) and the Grand canonical Monte Carlo (GCMC) were performed by GULP (Gale 1997). The C–S–H model in the present study is constructed according to the procedures proposed by Pellenq et al. (2009). Firstly, the layered analogue mineral of C–S–H, tobermorite 11 Å without water, was taken as the initial configuration of C–S–H model (Selvam et al. 2009). The initial configuration of the tobermorite 11 Å is shown in Fig. 1a, and the cell parameters of a , b , c , α , β and γ are 11.16, 7.39, 22.77 Å, 90°, 90° and 90°, respectively. In the simulation, the supercell of C–S–H model contains $2 \times 3 \times 1$ crystallographic unit cell of tobermorite 11 Å. The double layer models are created by cleaving the crystal structure at the center of the interlayer region that is parallel to the (001) crystallographic plane. The cleave line is along the interlayer calcium atoms and only exposes bridging silicate tetrahedrons on the surface. Ten models were built with interlayer distance from 13 to 22 Å. Silicate chains are then broken to match the Q species distribution obtained from NMR test (Chen et al. 2004). The dry disordered structure is plotted in Fig. 1b.

Subsequently, the GCMC method was utilized to investigate the structure of the dry calcium silicate skeleton emerged in water solution (Bonnaud et al. 2012). The dry sample obtained by cleaved tobermorite crystal was utilized for simulation. GCMC simulations determined the properties of the water molecules confined in the calcium silicate system at constant volume V in equilibrium with a fictitious infinite reservoir of liquid bulk water solution, imposing its chemical potential $\mu = 0$ eV and its temperature $T = 300$ K (Pellenq et al. 2009). The simulation process is analogous to water adsorption in the microporous phases, such as calcium silicate hydrate and zeolite (Puibasset and Pellenq 2008). The simulation included 300,000 circles for the system to reach equilibrium followed by 100,000 circles for the production run. For each circle, attempts were made to insert, delete, displace and rotate water molecules 1000 times in the constant volume calcium silica hydrate system (Bonnaud et al. 2012). When the simulation system reached equilibrium, the number of interlayer water molecules was recorded. As shown in Fig. 1c, with increasing pore size from 13 to 22 Å, the number of water molecules

increased from 92 to 246 and the average density for the interlayer water varied from 0.9 to 1.1 g/cm³. In the very narrow silicate channels (<16 Å), the solvated calcium atoms occupy the space for the water molecules, which reduced the density of water molecules. H-bonds connections between the water molecules and structural oxygen atoms densified water distribution.

Finally, molecular dynamic simulations under constant pressure and temperature (NPT) for 300 ps gave the structures of C–S–H gel at equilibrium states. The time step for the numerical integration of the Newtonian equations of motion for the system of N atoms was 0.1 fs, which is small enough to characterize the hydrogen bond dynamics of water molecules. For each case, further 1000 ps NPT run were employed to achieve the equilibrium configuration for structural and dynamic analysis.

The CSHFF force field (Shahsavari et al. 2011), developed for cement-based material, is utilized to simulate the C–S–H gel at different humidity states. The force field has been widely used in C–S–H simulations and proven competent to describe the structure, energy and mechanical properties of various calcium silicate phases (Pellenq et al. 2009; Youssef et al. 2011; Ji et al. 2012; Bonnaud et al. 2012; Manzano et al. 2011). The force field parameters of Ca, Si, O and H can be achieved from Shahsavari (2011). The Coulomb energy was computed using the Ewald summation technique with the following parameters: $\kappa = 0.24$ Å⁻¹ for the model and a minimum of $k_{\max} = 5$ for the each systems (κ is the width of the Gaussian charge distribution surrounding each charge and k_{\max} is the maximum number of k -vector in the reciprocal space in the direction corresponding to the smallest box dimension in the real space, $L = \|\vec{a}\|$, $\|\vec{b}\|$, or $\|\vec{c}\|$). The maximum k -vectors in the two other reciprocal space directions (k'_{\max} and k''_{\max}) have been added or removed with respect to the real space length of the two other box dimensions (L' and L''): $k'_{\max} = k_{\max} \times L'/L$ and $k''_{\max} \times L''/L$.

3 Molecular structure

3.1 Atomic intensity

Three simulated C–S–H gel samples with interlayer distance 13, 15 and 20 Å are shown in Fig. 2. The intensity profiles of different atoms in the three states are plotted in Fig. 3 versus the distance in z direction. The combination of the information in Figs. 2 and 3 gives a good understanding of the molecular structures of C–S–H gel samples. In all the samples, along z direction, the alternative maximums of Ca_w (interlayer calcium atoms), O_s (oxygen atoms in the silicate chains) and O_w (oxygen atoms in water molecules) in density profiles, as shown in Fig. 2,

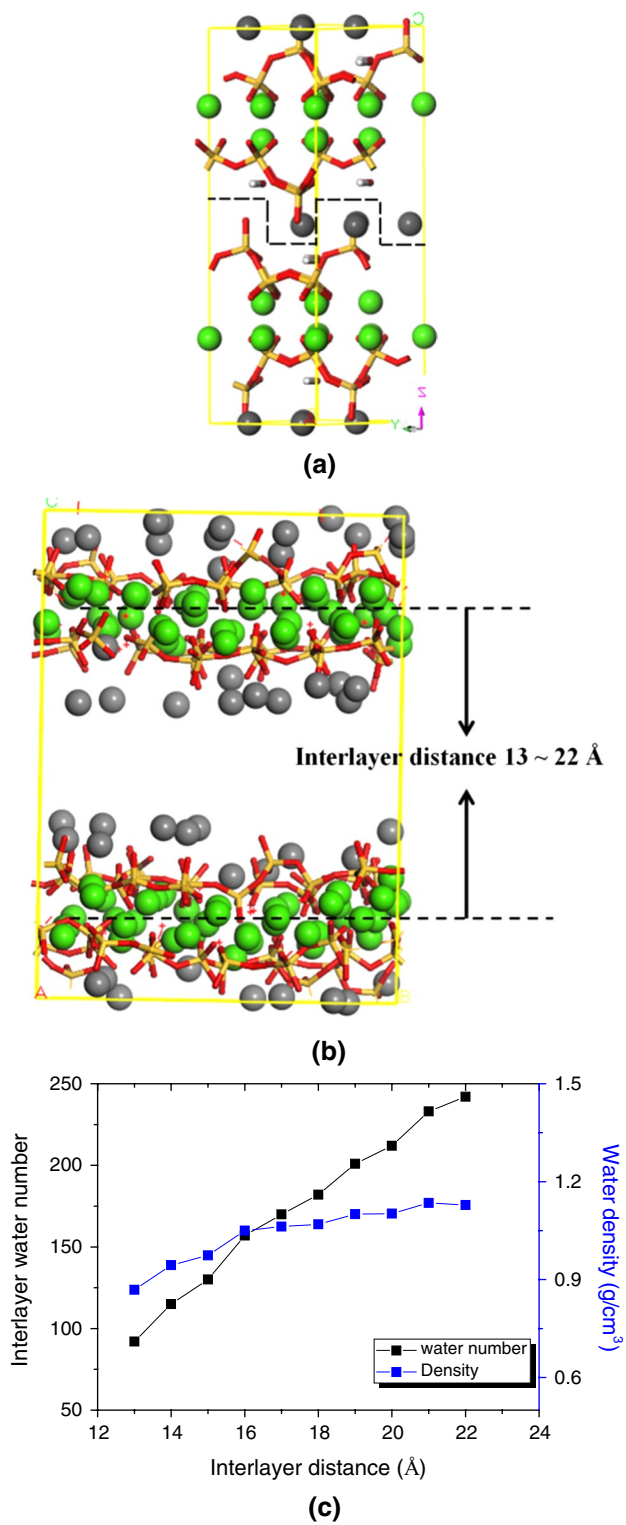


Fig. 1 **a** Tobermorite 11 Å and the cleavage line for the double-layer model. **b** Initial dry C-S-H structure for water adsorption simulation. Simulation box size: $a = 21.3$, $b = 21.2$, $c = 22.9 \sim 32.9$ Å; $\alpha = 90^\circ$, $\beta = 90^\circ$, $\gamma = 90^\circ$. The sticks represent the silicate chains (Si-O_s); the balls are corresponding to the calcium atoms (Ca_w and Ca_s)

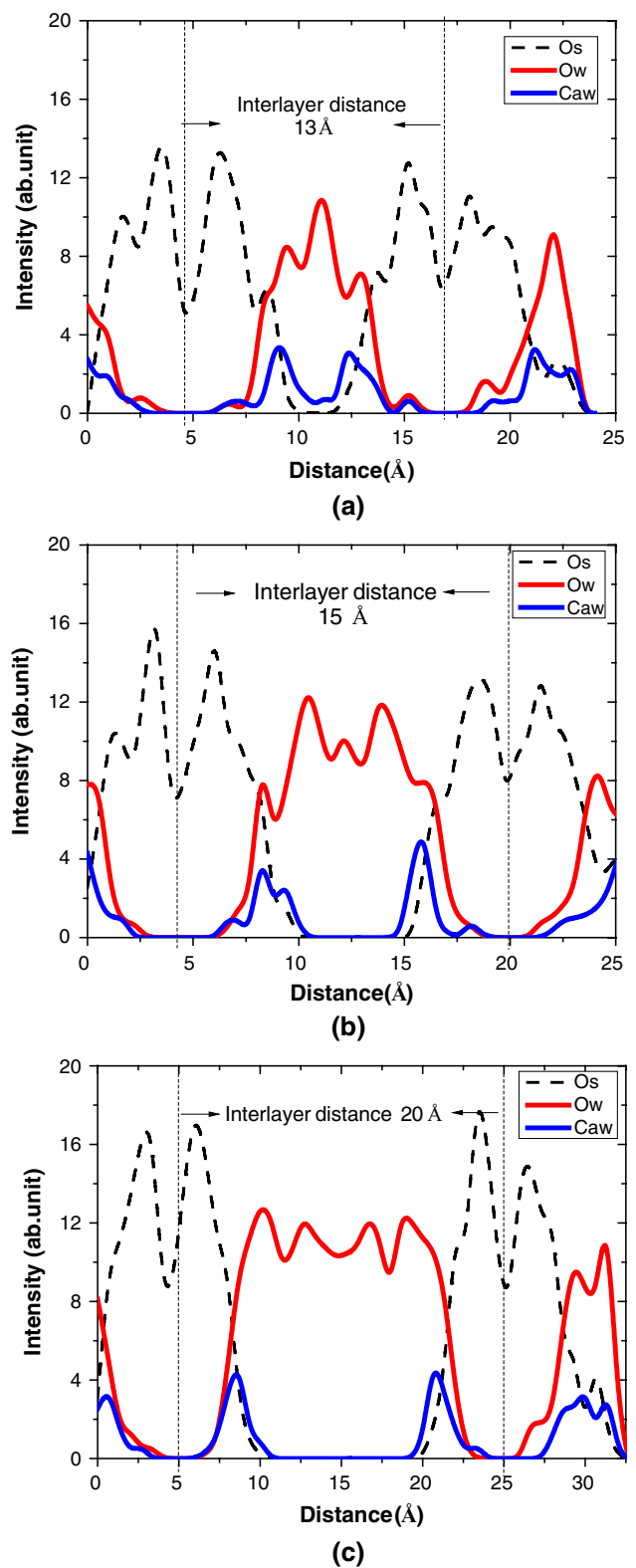


Fig. 2 Atomic density profile along z direction for the C-S-H gel with interlayer distance **a** 13 Å, **b** 15 Å and **c** 20 Å

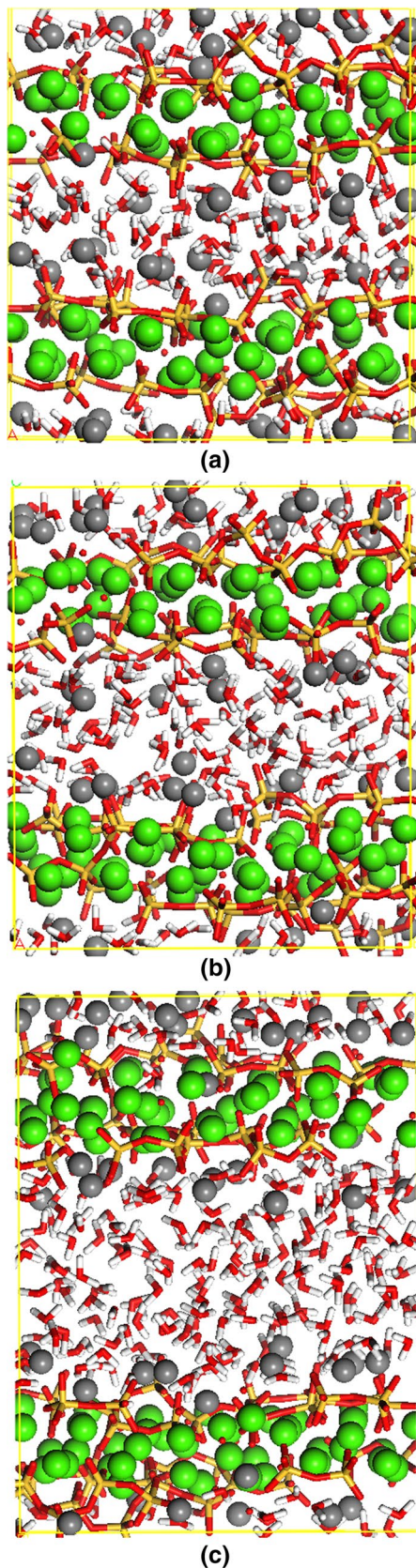


Fig. 3 Molecular structure of C–S–H gel with interlayer distance **a** 13 Å, **b** 15 Å and **c** 20 Å

imply that C–S–H gel has sandwich-like structure. It can be clearly observed in Fig. 3 that Ca_s and O_s (oxygen atoms in the silicate structure) form $\text{Ca}_s\text{--O}_s$ octahedrons and construct the Ca_s sheet; defective silicate chains graft on both sides of the Ca_s sheets; between the neighboring calcium silicate sheet distribute Ca_w and water molecules. The intensity of O_w distributes across the O_s distribution along z direction, meaning that water molecules are not only present in the interlayer regions but also diffuse into the defective region of calcium silicate sheet. The neighboring defective silicate chains can form transport channels where water can diffuse between. The multi-peaks distribution of water molecules indicates the disordered organization of interlayer water molecules. With increasing interlayer distance, the number of the water layers gradually increase and the location of the most intense peak shifts from the central of the pore to the surface of calcium silicate sheet. Under all these cases, positions of the O_w maximum are close to that of Ca_w and O_s , indicating that the water organization is disturbed by the calcium silicate substrates. In addition, the intensity of Ca_w exhibits a maximum near the O_s , and no Ca_w atoms are observed in the central of the pore, indicating the strong attraction between the $\text{Ca}_w\text{--O}_s$ connections.

Interlayer water organization is well described by the atomic density contours projected in the surface plane. The triangular trajectories of Si–O tetrahedron are used as the reference positions for analysis, and the trajectories of the water molecules located from 5 to 15 Å in the O_w intensity are recorded in Fig. 4. The red and black trajectories, representing silicon and interlayer calcium atoms, are taken as the reference positions for the water trajectories. With few trajectories overlapping two neighboring water molecules in different silicate channels, as shown in Fig. 4a, it is apparent that the mobility of channel water is relatively slow and no position exchange occurs. Most trajectories of water in this layer resemble those of silicon atoms that are the solid skeleton of C–S–H gel, implying the “immobile” characteristic of the water deeply embedded in the calcium silicate sheet. The motion of water molecules is the vibration at the fixed positions. In the upper layer (Fig. 4b), water molecules are concentrated near the Si and the Ca atoms, indicating the strong electronic interaction between water molecules and Ca, O_s atoms. At the distance from the Ca and the silicate tetrahedron, the contours become less ordered and exchanges between the water molecules occur more frequently. The third density map (Fig. 4c) exhibits the arrangement of the surface water. The atomic trajectories from the bottom to the top layers appear to show that water molecules transform from “immobile” to the “mobile” state.

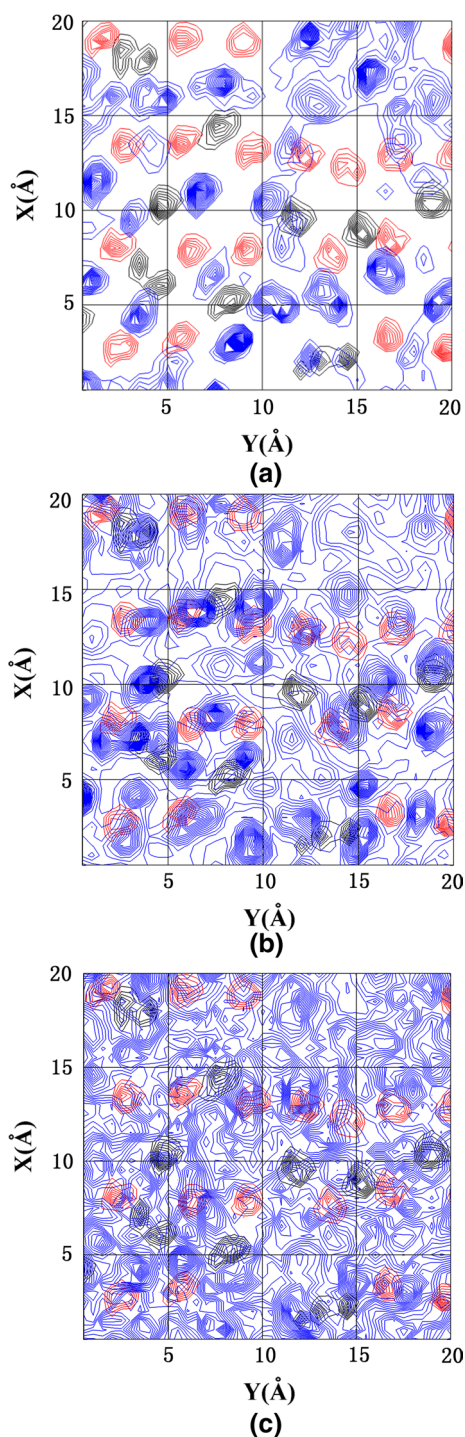


Fig. 4 Atomic density contours of C-S-H gel with interlayer distance 20 Å **a** $z = 5\text{--}10$ Å, **b** $10\text{--}12.5$ Å and **c** $12.5\text{--}15$ Å

3.2 Orientation profile

Orientation profiles, describing the dipole angle (φ_d) variation with distance from surface, give a better understanding of the water molecule structure in the complicated

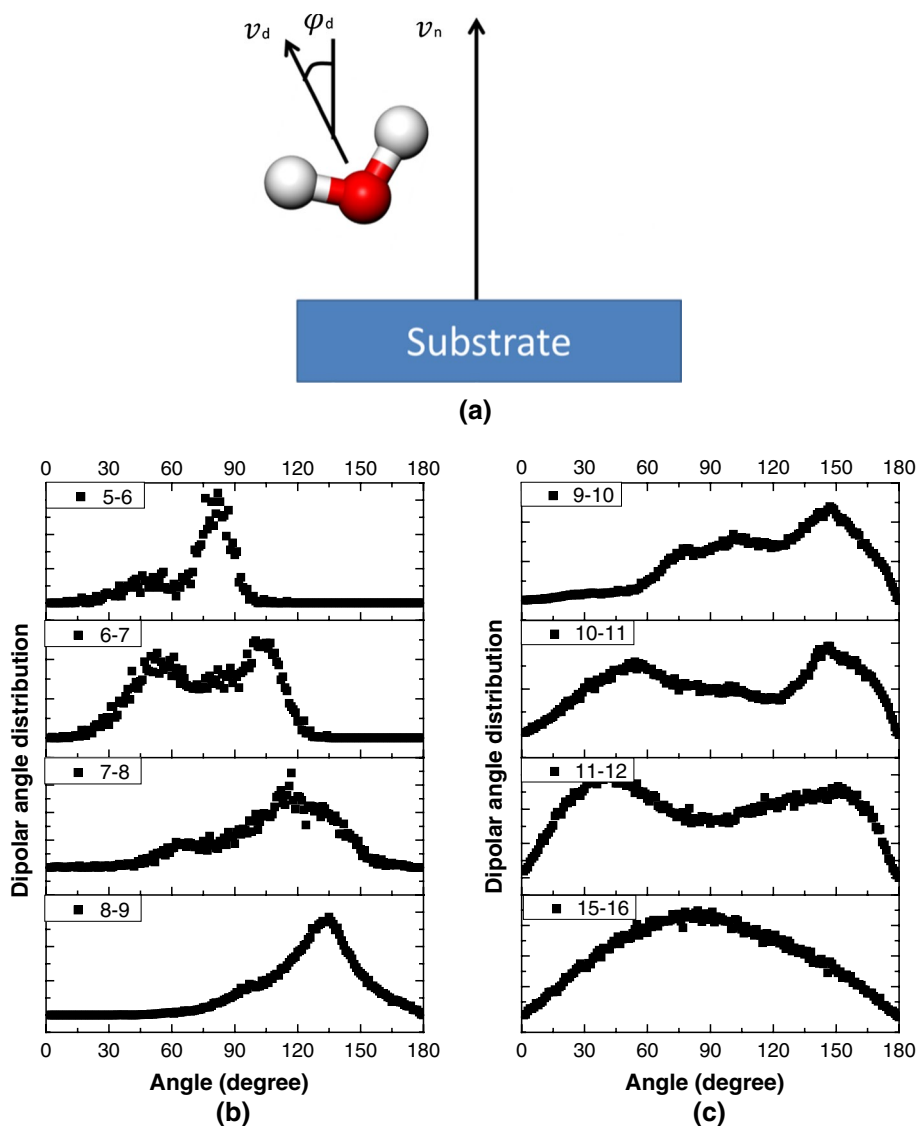
interface environment. In Fig. 5a, φ_d is the angle between the dipole vector (\mathbf{v}_d) of single water and the normal vector (\mathbf{v}_n) for the surface. The instantaneous orientations of water molecules at different layers indicate differing tendencies that can then be utilized to analyze the surface influence.

From the calcium silicate surface, the orientation distribution of the water molecules is calculated at 1 Å intervals and plotted in Fig. 5b, c, with the water layer located in the center of the pore taken for comparison. In the first layer ($z = 5\text{--}6$ Å), water molecules are, on average, deeply restricted between the silicate channel and are predominantly oriented with φ_d ranging from 80° , implying that dipole axis points parallel to the surface and slightly tilts away from the surface. In the second layer ($z = 6\text{--}7$ Å), the orientation profile has two major peaks located at around 53.7° and 104° , respectively. The bimodal distribution is attributed to the effects from O_s sites in the silicate chains and calcium atoms in calcium silicate sheet. The first peak ranging around 53.7° implies the dipolar vector pointing away from surface. The O_w atoms energetically prefer the calcium atoms, which contribute to small dipolar angle. The small dipolar angle distribution resembles that of type II water molecules on the Mg-OH and Ca-OH interface (Wang et al. 2004) ($\varphi_d = 30^\circ\text{--}60^\circ$). On the other hand, O_s atoms in the silicate chains result in the H_w -down orientation for water molecules, corresponding to the large dipolar angle distribution around 104° . From the previous simulation of interface between water molecule and hydroxylated silicate glass, water molecules have two ideal orientation styles with φ_d at 75° and 180° , respectively (Lee and Rossky 1994), and the water orientation in current simulation is close to the former style. As the water layer locates from 7 to 10 Å, the peak located at smaller angle disappears and the peak at large angle shifts from 114° to 147° , resulting from the highly concentrated O_s atoms in these layers. In particular, the more negative O_{NB} atoms accept the H-bonds from the surface water molecules. It can be observed in Fig. 5c that double peaks reappear in the layers located from 10 to 12 Å, suggesting that the concentration of interlayer calcium atoms is comparable with that of O_s atoms. Since the dipole angle of water molecules depends greatly on the frequent breakage of H-bonds between neighboring molecules, the water in the middle of the gel pore has no orientation preference.

3.3 Radial distribution function

With interlayer distance ranging from 13 to 22 Å, radial distribution functions (RDF) of $O_w\text{--}H_w$, $O_w\text{--}O_w$ and $H_w\text{--}H_w$ have been calculated and plotted in Fig. 6 describing the spatial correlation between water molecules. As shown

Fig. 5 **a** Schematic diagram of water orientation as measured by dipolar angle; **b** dipolar angle distribution of water layers (from $z = 5\text{--}6 \text{ \AA}$ to $z = 15\text{--}16 \text{ \AA}$)



in Fig. 6a, the first peak of oxygen–oxygen correlation shift from 2.98 to 2.78 Å and the width of the first peak distribution turns narrow, indicating that the C–S–H substrate can extend the $O_w\text{--}O_w$ correlation to larger distance. In the medium range, with increasing interlayer distance, the intensity of second and third maximum gradually decreases, and the distribution widens, which is accompanied by the weak spatial correlation of water molecules located at second and third shell. As the distance increases from 13 to 22 Å, the first maximum of RDF ($O_w\text{--}H_w$), which is related to the average H-bond number, gradually increases as shown in Fig. 6b. In the C–S–H gel, water molecules adsorbed near the calcium silicate sheet can donate H-bonds to the neighboring O_s atoms, reducing the

H-bond contribution from neighboring water molecules. Additionally, as compared with distribution in the larger pore, the third peak distribution is sharper, implying that the spatial correlation can maintain in longer distance, and the RDF ($H_w\text{--}H_w$) exhibits structural discrepancy at various interlayer distances. From Fig. 6c, the local minimum between first and second peak progressively decreases, while the peaks in the short range are more pronounced. The RDF curves of $O_w\text{--}O_w$, $O_w\text{--}H_w$ and $H_w\text{--}H_w$ of the bulk water are shown in Fig. 6d to compare with confined water. The RDF evolution indicates that the local structures of water molecules are strongly disturbed by the nanoconfinement and lose the tetrahedron feature as in the case of bulk water.

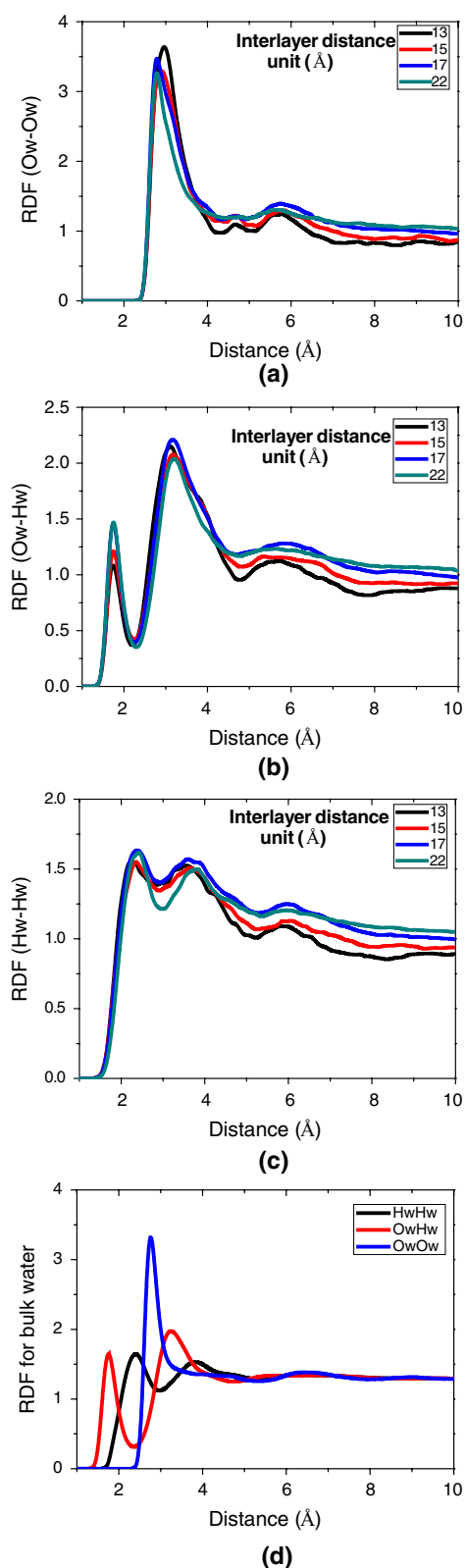


Fig. 6 Radial distribution function of **a** O_w-O_w , **b** O_w-H_w and **c** H_w-H_w at interlayer distance 13, 15, 17, 22 Å; **d** radial distribution function for the bulk water molecules

4 Dynamical properties

4.1 Mean square displacement

The mean square displacement $MSD(t)$ and diffusion coefficient (D) (Kerisit and Liu 2009), the parameters to estimate the dynamic properties of water molecules, can be defined by Eqs. 1 and 2,

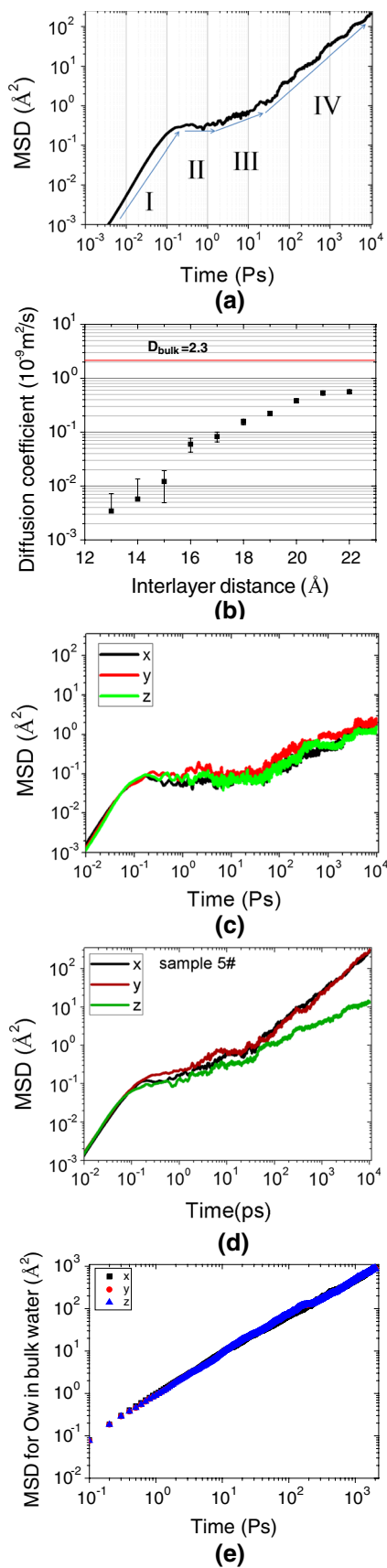
$$MSD(t) = \langle |\mathbf{r}_i(t) - \mathbf{r}_i(0)|^2 \rangle \quad (1)$$

$$2D \cdot t = \frac{1}{n} \langle |\mathbf{r}_i(t) - \mathbf{r}_i(0)|^2 \rangle \quad (2)$$

where $\mathbf{r}_i(t)$ represents the position of atom i at time t , $\mathbf{r}_i(0)$ is the original position of atom i . MSD takes into account three-dimensional coordinates for the bulk water molecules in x , y and z directions, two-dimensional coordinates parallel to the C-S-H substrate and one-dimensional coordinate perpendicular to the C-S-H substrate.

Figure 7a represents four stages of the time dependence of MSD for C-S-H gel with interlayer distance 17 Å. Ballistic motion $\langle r^2 \rangle \sim t^2$ dominates as time shorter than 0.2 ps, implying the inertia behavior of atoms at short time. During 0.2–2 ps, $\langle r^2 \rangle$ leads to nearly a plateau and at longer diffusion times with $\langle r^2 \rangle \sim t^\beta$. The diffusion stage can be further decomposed into anomalous diffusion with $\beta < 1$ and normal diffusion with $\beta = 1$. As shown in Fig. 7c, the plateau is around 100 ps for the case of interlayer distance 13 Å, indicating the glassy nature of interlayer water molecules in the ultra-confinement. It should be noted that the confinement effect is significant in case of nanopore with size less than 10 Å. Youssef investigated the structural water molecules strongly rooted in the interlayer region (~ 10 Å). After the 400 ps cage stage plateau, the MSD step into the diffusion region (Youssef et al. 2011). At larger pore and infinite region, as shown in Fig. 7d, e, the diffusion stage is directly following the ballistic regime without presence of cage stage. It means that the water confined in the larger pores transform into the liquid state.

Figure 7b shows the interlayer distance dependence of diffusion coefficients that are derived from the mean square displacement. While the interlayer distance increases from 13 to 22 Å, the diffusion coefficient increases from 0.00342 to $0.53 \times 10^{-9} \text{ m}^2/\text{s}$ ($0.0014 \times D_{\text{water}}$ to $0.23 \times D_{\text{water}}$, D_{water} corresponding to the diffusion coefficient of bulk water). It should be noted that even though the pore size changes only 1 nm, the diffusion coefficient transfers through three orders of magnitude. The sensitivity of the diffusion coefficient in the pore size range is due to heterogeneous dynamics of water molecules confined in the nanopores. It is the



◀**Fig. 7** **a** Mean square displacement of C–S–H (interlayer distance 17 Å) evolution from 0.01 to 10000 ps; **b** diffusion coefficient for C–S–H gel with interlayer distance from 13 to 22 Å; **c** and **d** x, y and z component of MSD for C–S–H with interlayer distance 13/20 Å; **e** MSD for the O_w atoms in bulk water

first time to report the quantitative estimation of the pore-size-dependent dynamics of confined water molecules. The diffusion and porous geometry relation can be employed to characterize the transport behavior of water and ions in the C–S–H gels with various nanopores by the multi-scale method (Ma et al. 2014). Additionally, the geometric-dependent properties further supplement the understanding of the dynamics of the water in cement-based materials. The component-dependent dynamics has been illustrated by studying C–S–H substrates with different Ca/Si ratio (Qomi et al. 2014). The simulation results indicated that diffusivity increases with Ca/Si ratio. Behind the phenomenon is the mechanism that the bridging silicate tetrahedron in the silicate channel, varying with chemical composition, influences the motion behavior of interlayer water molecules. By using the ¹H nuclear magnetic resonance, the water in C–S–H gels was distinguished and categorized into three types normally: chemically bound water that is incorporated into the structure and forms strong chemical bond with the calcium silicate structure, physical bound water that is deeply adsorbed near the surface and capillary water that is not bound and diffuses freely in the capillary pores.

The MSD_x and MSD_y, parallel to the pore, and MSD_z, normal to the pore, are shown in Fig. 7c, d. When the interlayer distance is 13 Å, the MSD curve normal to the pore resembles those parallel to the pore. Both MSD curves exhibit a long plateau, indicating that width of the pore is so narrow that the traveling channel is significantly influenced by the protruded silicate tetrahedron and the interlayer calcium atoms. On the other hand, as shown in Fig. 7d, for the water confined in the larger pore, in the diffusion regime, the MSD_z gradually deviates from those parallel to xy plane and exhibits low mobile ability. The discrepancy between three-dimensional diffusion coefficients results from the enhanced connectivity at the situation of larger pore size.

4.2 Vibration spectrum

Spectra of the atomic motions in the translational, librational and vibrational frequency allow further characterization of the simulation model in dynamical respect. Infrared absorption can be detected if the dipole momentum μ in a molecule is changed during the normal vibration. The intensity of an infrared absorption band depends on the change of the dipole moment μ during this vibration. The

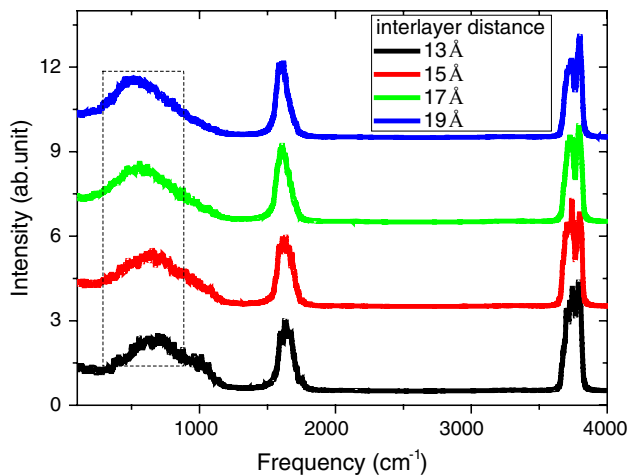


Fig. 8 Simulated IR spectrum of water molecules confined in the pores with interlayer distance from 13 to 22 Å

infrared absorption spectrum can be calculated by Fourier transformation of the dipole moment autocorrelation function (Praprotnik et al. 2004), shown in Eq. (3).

$$I(\omega) \propto \int_0^{\infty} \langle M(t) \cdot M(0) \rangle \cos(\omega t) dt \quad (3)$$

where $I(\omega)$ is the spectral density, $M(t)$ is the total dipole moment of the system at time t and ω is the vibration frequency. $M(t)$ is the sum of all the individual dipole moments μ of water molecules.

The autocorrelation function of the dipole moment is expressed by Eq. (4)

$$\langle M(t) \cdot M(0) \rangle = \left\langle \sum_{j=1}^n e_j r_j(t) \cdot \sum_{j=1}^n e_j r_j(0) \right\rangle \quad (4)$$

where n is the number of all the atoms in the system, e_j is the electric charge of the j th atom and $r_j(t)$ is the position vector of the j th atom at time t . The angular brackets represent the average over all the time origin.

Figure 8 demonstrates the calculated IR spectra of water molecules in pores with different sizes. The double peak at 3740 cm^{-1} corresponds to the normal modes of vibration of a water molecule describing the antisymmetric and symmetric bond stretches. The single peak at $1600\text{--}1633 \text{ cm}^{-1}$ represents the angle bending normal mode of a water molecules. The IR banding distributed from 300 to 900 cm^{-1} arises from to the librational and translational motion of water molecules. The simulated spectrum matches well with the IR spectrum by experimental findings (Yu et al. 1999). Furthermore, as shown in Fig. 8, with increasing interlayer distance, the spectrum distribution in the order of 3740 cm^{-1} remains unchanged, while the distributions at lower frequency

domains shift toward lower values. This response infers that the interlayer geometry has little influence on the stretching vibration but has great effect on the bending, librational and translational motions. It should be noted that all the vibrational bands' water arise from contributions from different components from water molecules in different hydrogen-bonded environments (Kitadai et al. 2014). Similar vibration spectrum variation trend has been observed in other layer minerals. The vibrational modes of interlayer water molecules in the $\text{Ca}_2\text{Al}\text{--Cl}$ LDH were investigated in previous research (Kirkpatrick et al. 2005). In comparison with those of bulk water, the translational motions of interlayer water molecules are located in the domain with higher frequency. The lower frequency can be attributed to the stronger H-bonds network in the small pore system, which can be explained in the following bond stability section.

4.3 Bond stability

As previously noted, the nearest neighbor of interlayer water molecules are composed of structural oxygen atoms in the silicate chains, the interlayer Ca atoms and the surrounding water molecules. Hence, the $\text{Ca}\text{--O}_w$, $\text{O}_w\text{--O}_w$ and $\text{O}_s\text{--O}_w$ are the major chemical bonds bridging the neighboring water molecules and calcium silicate sheet. The stability of the chemical bonds between water molecules and neighboring atoms determines the mobile capability of interlayer water molecules. As in previous research studying the H-bond strength (Youssef et al. 2011), the time correlated function (TCF) is utilized to describe dynamical properties of various chemical bonds. TCF of a bond is represented in Eq. (5):

$$C(t) = \frac{\langle \delta b(t) \delta b(0) \rangle}{\langle \delta b(0) \delta b(0) \rangle} \quad (5)$$

where $\delta b(t) = b(t) - \langle b \rangle$, $b(t)$ is a binary operator that takes a value of one if the pair (e.g., $\text{Ca}\text{--O}$) is bonded and zero if unbonded, and $\langle b \rangle$ is the average value of b over all simulation time and pairs. The chemical bonds break and reform during the time evolution, which result in the connectivity variation in C–S–H gel. If the connectivity persists unchanged, the TCF of bonds will maintain constant value one. Otherwise, the break of bonds lead to lower TCF, and the more frequent the bond breakage, the lower value of TCF. By comparing the deviations from one in the TCF curves, the stability of various bonds can be estimated.

Figure 9 indicates that the TCF of chemical bonds of $\text{Ca}\text{--O}_w$, $\text{O}_w\text{--O}_s$ and $\text{O}_w\text{--O}_w$ exhibit different bond strength. According to the reduction degree of the $C(t)$ values, the bond strength ranks in the following order: $\text{Ca}\text{--O}_w > \text{O}_w\text{--O}_s > \text{O}_w\text{--O}_w$. For $\text{Ca}\text{--O}_w$ bond, the TCF curves remain almost constant at 0.9 after the reduction during 0.2 ps,

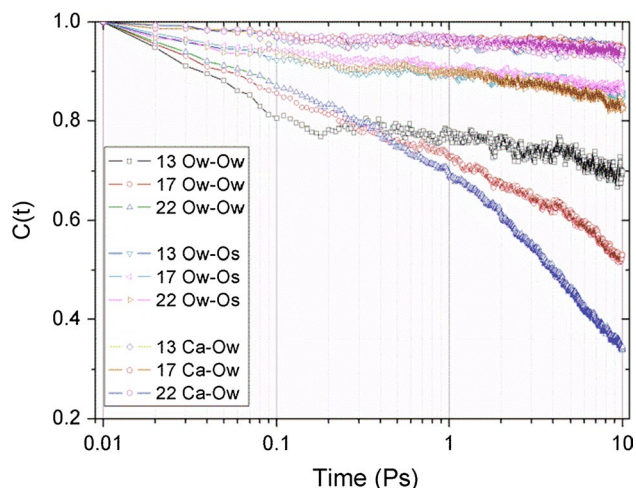


Fig. 9 Time correlated function of Ca–O_w, O_w–O_s and O_w–O_w connection for the water molecules in C–S–H gel with interlayer distance 13, 17 and 22 Å

indicating stable connectivity. The H-bond connection between O_s in the silicate chain and the O_w is slightly weaker than the Ca–O_w bond, and the TCF of O_w–O_s gradually decreases to 0.8 at 10 ps. In addition, TCF of O_w–O_s and Ca–O_w bonds exhibit slight influence from the pore geometry. The high strength of these bonds imposes a rigid cage stage in the translational dynamics for the water molecules. The bond stability of O_w–O_w H-bonds is, however, significantly weakened as the interlayer distance increases. In the small pore, the TCF first decreases quickly during 0.2 ps and then reaches a plateau as in the curves of O_w–O_s and Ca–O_w bonds. With increasing pore size, the plateau or the slow decreasing regime disappear and the correlation function decays rapidly, implying the weak H-bond connection in the larger nanopores. TCF evolution from small to large pore reflects that interlayer water transforms from glass to liquid state in the respect of dynamic behavior.

4.4 Van Hove function

The self-part of van Hove function assists in understanding the dynamical properties of water confined in the C–S–H gel. The function can be expressed in Eq. 6.

$$G_s(r, t) = \frac{1}{N} \sum_{j=1}^N \langle \delta(r - |r_j(t) - r_j(0)|) \rangle \tag{6}$$

The physical meaning of $2\pi r G_s(r, t)$ is the probability that particle i has moved a distance of r with escaping time t . Figure 10a, b demonstrates the van Hove functions

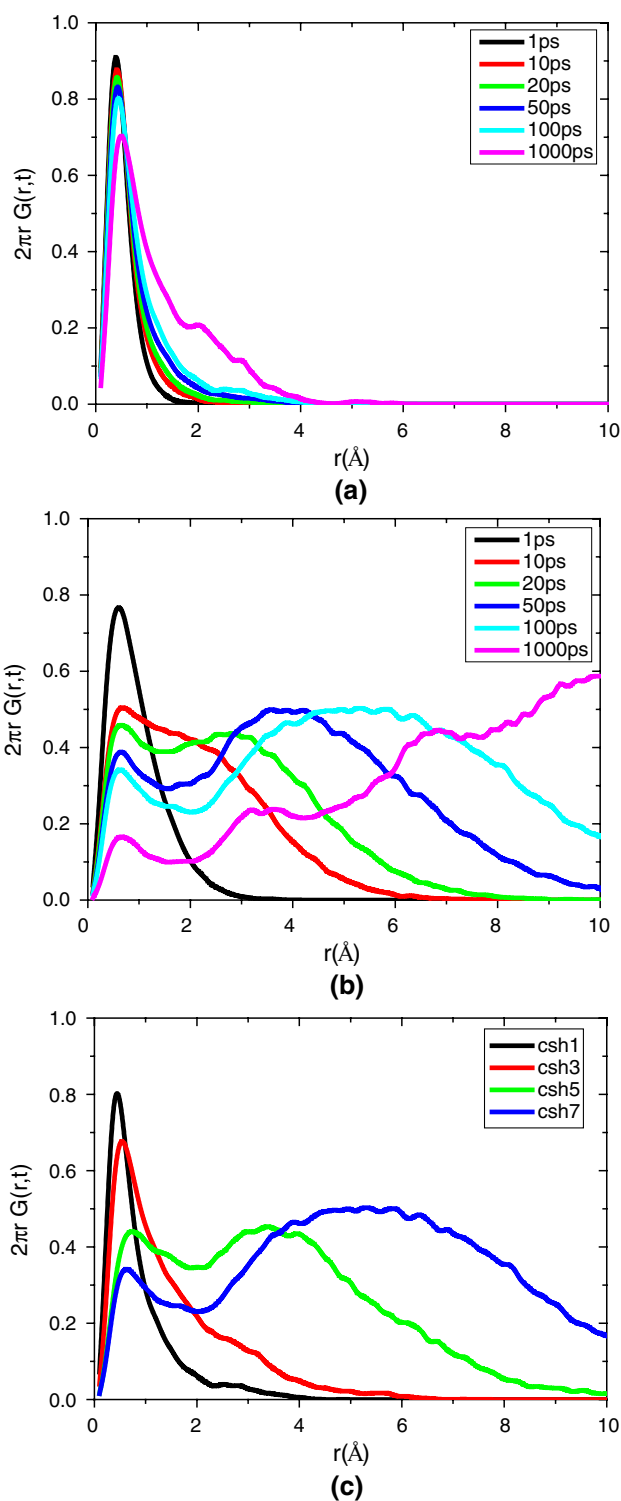


Fig. 10 Self-part of van Hove function for water molecules confined in C–S–H gel with **a** interlayer distance 13 Å; **b** interlayer distance 20 Å at different simulation time; **c** water molecules confined in the interlayer region of 13, 15, 17 and 20 Å

of water confined in C–S–H gel with small and large sizes at different times. From Fig. 10b, at short time ($t < 1$ ps), only one peak occurs at $r < 2$ Å, while at longer timescale ($t > 20$ ps), another peak is located at around $r = 3$ Å. When the time reaches as long as 1000 ps, the third peak located at $r = 7$ Å occurs. The first peak corresponds to the cooperative rearrangement and indicates that the water molecules are constrained in the cage. A second peak in $G_s(r, t)$ has been observed in some glass-forming liquids and supercooled liquid, which can be interpreted as single water molecule hopping. The hopping process describes that water molecules stay localized in their cage for a while and subsequently escape from the cage approximately one intermolecular distance. In contrast to the case of water confined in pore with larger size, the water molecules with ultra-confinement exhibit pronounced cage effect. When the time is larger than 1000 ps, the van Hove function demonstrates one small shoulder from 2 to 4 Å, which means that increasing number of water molecules escape from the cage. Figure 10c shows the van Hove function of water confined in gel pores with different size at 100 ps. In the small pore, the van Hove function is limited in the cage radius (2 Å). As discussed in the structural section, the motions of water molecule in smaller pore are highly restricted by the O_{NB} sites in the silicate chains and interlayer Ca atoms. In respect of energy, the hopping behavior of water molecules is closely related to the hopping energy barrier. With increasing pore size, the stable O_w-O_s H-bond and Ca_w-O_w connections are gradually replaced by the unstable O_w-O_w H-bond. Hence, the water molecules are able to overcome the energy barrier from confinement and diffuse to the second hopping site and even the third hopping site.

The hopping mechanism for the interlayer 20 Å can be explained by monitoring the movement of water molecules in the interfacial region. With increasing distance from C–S–H substrate, the moving ability of water molecules gradually increase, which categorize the water molecules into an “immobile” and “mobile phase.” Different phases can exchange with each other. Figure 11 shows the surface water molecules highly adsorbed by the non-bridging oxygen site and calcium atoms gradually escape from the cage and depart from the substrate. Due to the heterogeneous dynamics of surface water and pore water, even at long time stage, part of water molecules are still confined in the substrate, part of water molecules freely diffuse and part of water molecules exchange between immobile and mobile states. The multi-peaks in the van Hove functions can be observed.

5 Mechanical properties

The structure and motion of interlayer water molecules influence the mechanical performance of the C–S–H gel.

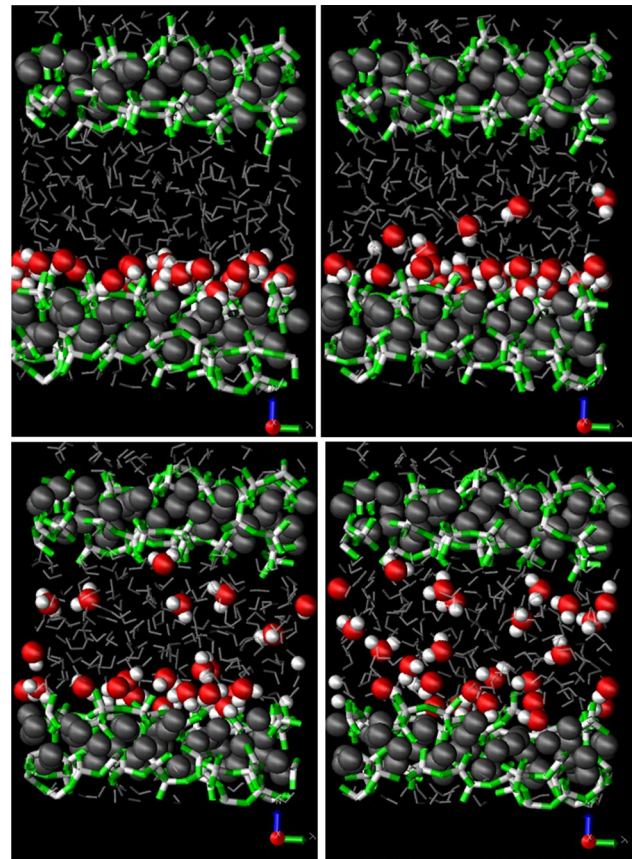


Fig. 11 Water molecules adsorbed in the interfacial region diffuse from surface

In order to investigate the cohesion force at different interlayer distance, the internal fluid pressures are calculated as the following Eqs. 7 and 8:

$$P_f = \frac{1}{V} \sum_{a=1}^N \sum_{b \neq a}^N S_{ab} \quad (7)$$

$$S_{ab} = - \left[mv_a v_b + \frac{1}{2} \sum_{n=1}^{N_p} (r_{1a} F_{1b} + r_{2a} F_{2b}) + \frac{1}{2} \sum_{n=1}^{N_b} (r_{1a} F_{1b} + r_{2a} F_{2b}) + \frac{1}{3} \sum_{n=1}^{N_a} (r_{1a} F_{1b} + r_{2a} F_{2b} + r_{3a} F_{3b}) + kspace(r_{ia} F_{ib}) \right] \quad (8)$$

The stress tensor S_{ab} between atom a and b is composed of kinetic energy contribution in first term, pairwise interaction in the second term, bond energy interaction in the

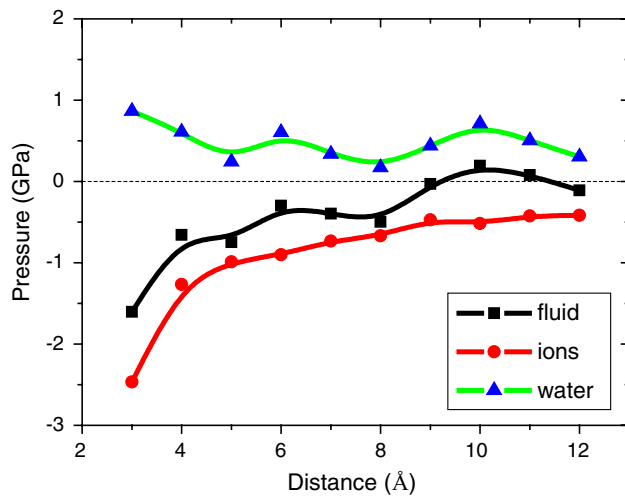


Fig. 12 Fluid pressure evolution with interlayer distance

third term and Coulombic interaction in the final term. In addition, the internal fluid pressure can be further decomposed into the contribution from water molecules (P_w) and interlayer calcium atoms (P_{Ca}). The fluid pressure evolution as a function of interlayer distance is shown in Fig. 12. And it can be observed that from all the cases under study, the positive pressure from the water molecules indicates the disjoining role. On the other hand, the highly negative pressure of the calcium ions contributes to the cohesive force in the C–S–H gel. The negative pressure is mainly driven between the calcium atoms and the non-bridging oxygen sites in the defective silicate chains. In this respect, with increasing interlayer distance, part of O_s –Ca– O_s bonds are gradually substituted by the O_w –Ca– O_w connections and increasing number of water molecules become the hydration shell of interlayer calcium atoms. It results in the cohesive pressure reduction from 1.5 to <0.2 GPa. The cohesive pressure matches well with the fracture strength (~1 GPa) simulated by the “realistic model” (Pellenq et al. 2009). The disjoining pressure can explain the hygral volume change of cement-based materials thermodynamically. At high humidity, water molecules penetrate into the interlayer region and build up the swelling pressure. It should be noted that high concentrations of interlayer Ca atoms and non-bridging oxygen sites can contribute to large amount of water adsorption, accumulating higher swelling pressure and increasing the interlayer distance. This necessarily leads to an increase in the macroscopic volume.

Current finding from Monte Carlo method (Bonnaud et al. 2012) suggests that the interaction between solid surface and fluid has been investigated for many years. The term disjoining pressure is used to describe the complex interaction between water and two solid surfaces. The measurable disjoining pressure is generated by a superposition of attractive and repulsive forces. The attractive

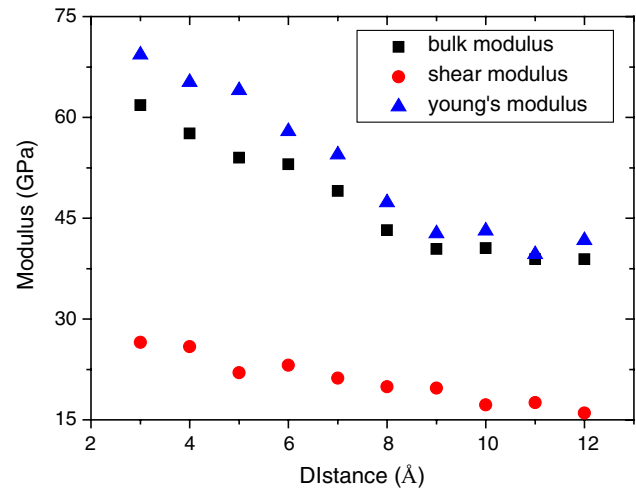


Fig. 13 Modulus evolution with increasing distance

dispersive or molecular forces are in the first place van der Waals forces. The van der Waals attraction is weakened by adsorbed water films. The diffuse electric double layer is at the origin of a repulsive component. The third term, the structural term, includes the effect of solvation or hydration shells. The oscillation of the disjoining fluid pressure in C–S–H gel can be attributed to three respects: (1) the effect of the disordered hydrophilic calcium silicate sheets that offer a significant number of acceptor sites for hydrogen bonds to the confined water, (2) the strong interlayer calcium solvation effects and (3) the ultra-confinement effect from the 1–2 nm pore.

The moduli of C–S–H gel with different interlayer distances have been calculated and presented in Fig. 13. As the interlayer distance increases from 13 to 22 Å, the bulk modulus of C–S–H gel gradually decreases from 62 to 38 GPa and shear modulus reduces from 28 to 15 GPa, implying that the nanoporosity has significant influence on the mechanical behavior of the C–S–H gel. The bulk modulus is close to the value of C–S–H gel (31 GPa) that is obtained from nanoindentation test (Costantinides and Ulm 2004). The weakening modulus can be interpreted by the combination of structural and dynamical results in previous section. With increasing water content, the O_w – O_s and Ca– O_w connections with strong bond strength are gradually replaced by the unstable O_w – O_w connections. However, the diffusion coefficient of water molecules significantly increases at larger interlayer distance. This can be interpreted as the enhancement of viscosity. While the interlayer water molecules transform from glassy state to liquid state, the bond stiffness of C–S–H gel is significantly weakened. Interestingly, the mechanical properties of many silicate materials are reduced, as they are immersed in water, which is called hydrolytic weakening effect. The weakening phenomena are explained in respect of chemical reactions, the silicate

network transformation and water dissociation in previous research (Hou et al. 2014a, b). The glass–liquid transition for the interlayer water molecules is another reason for the hydrolytic weakening, in particular for the materials in the high humidity condition.

6 Conclusions

The structures, dynamics and mechanical properties of water molecules confined in the nanopores with interlayer distance from 13 to 22 Å have been investigated in light of the molecular dynamics. The following conclusions are presented.

1. The water molecules near the C–S–H surface are strongly influenced by the O_{NB} atoms in the silicate chains and Ca_w atoms in the interlayer region. They demonstrate the following structural features: layering in the water density profile, the orientation preference in the dipolar angle distribution and long special correlation in the radial distribution function.
2. Dynamically, while the interlayer distance increases by 10 Å, the diffusion coefficient transfers through two orders of magnitude from 3.42×10^{-12} to 5.3×10^{-10} m^2/s^2 . In the mean square displacement (MSD) curves, the cage stage, a characteristic of the dynamics in the glasses, gradually disappears with increasing interlayer distance. The dynamic evolution of water molecules is primarily induced by the changes of the strength of H-bonds and Ca– O_w connections, which is consistent with lowering of the frequency in the simulated vibration spectrum. The strongly attractive interaction between water molecules and calcium silicate layer is weakened and the motion of water molecules is less restricted at large interlayer distance.
3. The cohesion in the C–S–H gel, contributed by the interlayer calcium atoms, progressively diminishes from 1.5 to 0 GPa, due to the enhancing disjoining effect of water molecules connected with calcium atoms with increasing interlayer distance.

Acknowledgments Technical support from the LAMMPS and GULP softwares, financial support from the China Ministry of Science and Technology under Grant 2015CB655100, Shandong Provincial Natural Science Foundation under Grant 2014ZRB01AE4 and National Natural science foundation of China under Grant 51508292 are gratefully acknowledged.

References

- Bonnaud PA, Ji Q, Coasne B, Pellenq RJ-M, Van Vliet KJ (2012) Thermodynamics of water confined in porous calcium–silicate–hydrates. *Langmuir* 28:11422–11432
- Bordallo HN, Aldridge LP, Desmedt A (2006) Water dynamics in hardened ordinary Portland cement paste or concrete: from quasielastic neutron scattering. *J Phys Chem B* 110:17966–17976
- Chen JJ, Thomas JJ, Taylor HFW, Jennings HM (2004) Solubility and structure of calcium silicate hydrate. *Cem Concr Res* 34:1499–1519
- Costantinides G, Ulm F (2004) The effect of two types of C–S–H on the elasticity of cement-based materials: result from nanoindentation and micromechanical modeling. *Cem Concr Res* 34(1):67–80
- Gale JD (1997) Gulp: a computer program for the symmetry-adapted simulation of solid. *J Chem Soc Faraday Trans* 93(4):629–637
- Greener J, Peemoeller H, Choi C, Holly R, Reardon EJ, Hansson CM, Pintar MM (2000) Monitoring of hydration of white cement paste with proton NMR spin–spin relaxation. *J Am Ceram Soc* 83(3):623–627
- Hou D, Ma H, Li Z, Jin Z (2014a) Molecular simulation of “hydrolytic weakening”: a case study on silica. *Acta Mater* 80:264–277
- Hou D, Ma H, Zhu Y, Li Z (2014b) Calcium silicate hydrate from dry to saturated state: structure, dynamics and mechanical properties. *Acta Mater* 67:81–94
- Ji Q, Pellenq RJM, Van Vliet KJ (2012) Comparison of computational water models for simulation of calcium silicate hydrate. *Comput Mater Sci* 53:234–240
- Kerisit S, Liu CX (2009) Molecular simulation of water and ion diffusion in nanosized mineral fractures. *Environ Sci Technol* 43:777–782
- Kirkpatrick RJ, Kalinichev AG, Wang J, Hou X, Amonette JE (2005) Molecular modeling of the vibrational spectra of interlayer and surface species of layered double hydroxides. *CMS Workshop Lect* 13:239
- Kitadai N, Sawai T, Tonoue R, Nakashima S, Katsura M, Fukushima K (2014) Effects of ions on the OH stretching band of water as revealed by ATR-IR spectroscopy. *J Solut Chem* 43(6):1055–1077
- Korb JP, Monteilhet L, McDonald PJ, Mitchell J (2007) Microstructure and texture of hydrated cement-based materials: a proton field cycling relaxometry approach. *Cem Concr Res* 37(3):295–302
- Lee SH, Rosky PJ (1994) A comparison of the structure and dynamics of liquid water at hydrophobic and hydrophilic surfaces—a molecular dynamics simulation study. *J Chem Phys* 100(4):3334–3345
- Li Z (2011) *Advanced concrete technology*. Wiley, Hoboken
- Ma H, Li Z (2013) Realistic pore structure of Portland cement paste: experimental study and numerical simulation. *Comput Concr* 11(4):317–336
- Ma H, Hou D, Liu J, Li Z (2014) Estimate the relative electrical conductivity of C–S–H gel from experimental results. *Constr Build Mater* 71:392–396
- Manzano H, Moeini S, Marinelli F, van Duin A, Ulm F, Pellenq R (2011) Confined water dissociation in microporous defective silicates: mechanism, dipole distribution, and impact on substrate properties. *J Am Chem Soc* 134(4):2208–2215
- Manzano H, Pellenq R, Ulm F, Buehler M (2012) Hydration of calcium oxide surface predicted by reactive force field molecular dynamics. *Langmuir* 28:4187–4197
- Pellenq R, Kushima A, Shahsavari R, Van Vliet KJ, Buehler MJ, Yip S (2009) A realistic molecular model of cement hydrates. *Proc Natl Acad Sci* 106(38):16102–16107
- Plimpton S (1995) Fast parallel algorithms for short-range molecular dynamics. *J Comput Phys* 117(1):1–19
- Plimpton S, Thompson A, Crozier P, Kohlmeyer A (2001) LAMMPS molecular dynamics simulator. <http://lammps.sandia.gov/index.html>. Accessed 18 Jan 2014

- Praprotnik M, Janezic D, Mavri J (2004) Temperature dependence of water vibrational spectrum: a molecular dynamics simulation study. *J Phys Chem A* 108(50):11056–11062
- Puibasset J, Pellenq R (2008) Grand canonical Monte Carlo simulation study of water adsorption in silicalite at 300 K. *Phys Chem B* 112(20):6390–6397
- Qomi MJA, Bauchy M, Ulm FJ, Pellenq RJM (2014) Anomalous composition-dependent dynamics of nanoconfined water in the interlayer of disordered calcium-silicates. *J Chem Phys* 140(5):054515
- Rakiewicz EF, Benesi AJ, Grutzeck MW, Kwan S (1998) Determination of the state of water in hydrated cement phases using deuterium NMR spectroscopy. *J Am Chem Soc* 120(25):6415–6416
- Selvam RP, Subramani VG, Murray S, Hall K (2009) Potential application of nanotechnology on cement based materials. Project Report MBTC DOT 2095/3004
- Shahsavari R (2011) Hierarchical modeling of structure and mechanics of cement hydrate. PhD thesis of Massachusetts Institute of Technology
- Shahsavari R, Pellenq RJM, Ulm FJ (2011) Empirical force fields for complex hydrated calcio-silicate layered materials. *Phys Chem Chem Phys* 13(3):1002–1011
- Wang PS, Ferguson MM, Eng G, Bentz DP, Ferraris CF, Clifton JR (1998) ^1H nuclear magnetic resonance characterization of Portland cement: molecular diffusion of water studied by spin relaxation and relaxation time-weighted imaging. *J Mater Sci* 33:3065–3071
- Wang JW, Kalinichev AG, Kirkpatrick RJ (2004) Molecular modeling of water structure in nano-pores between brucite (001) surfaces. *Geochim Cosmochim Acta* 68(16):3351–3365
- Youssef M, Pellenq RJM, Yildiz B (2011) Glassy nature of water in an ultraconfining disordered material: the case of calcium silicate hydrate. *J Am Chem Soc* 133:2499–2510
- Yu P, Kirkpatrick RJ, Poe B, McMillan PF, Cong X (1999) Structure of calcium silicate hydrate (C–S–H): near-, mid-, and far-infrared spectroscopy. *J Am Ceram Soc* 82(3):742–748